Biomaterials 269 (2021) 120641

Contents lists available at ScienceDirect

Biomaterials

journal homepage: www.elsevier.com/locate/biomaterials

Elastin-like hydrogel stimulates angiogenesis in a severe model of critical limb ischemia (CLI): An insight into the glyco-host response

Grazia Marsico [a], Chunseng Jin [g], Sunny A. Abbah [a], Eva M. Brauchle [e,f], Dilip Thomas [a], Ana Lúcia Rebelo [a], Doriana Orbanić [d], Sandrine Chantepie [h], Paolo Contessotto [a], Dulce Papy-Garcia [h], Carlos Rodriguez-Cabello [d], Michelle Kilcoyne [a,b], K. Schenke-Layland [e,f], N.G. Karlsson [g], Karl J.A. McCullagh [c], Abhay Pandit [a,*]

[a] CÚRAM SFI Research Centre for Medical Devices, National University of Ireland Galway, Galway H92 W2TY, Ireland
[b] Carbohydrate Signalling Group, Microbiology, School of Natural Sciences, National University of Ireland Galway, Galway H92 W2TY, Ireland
[c] Physiology Department, National University of Ireland Galway, Galway H92 W2TY, Ireland
[d] Bioforge, Ciber-BBN, The University of Valladolid, Spain
[e] Department of Women's Health, Research Institute for Women's Health, The Eberhard-Karls-University Tuebingen, Germany
[f] The Natural and Medical Sciences Institute (NMI) at the University of Tübingen, Reutlingen, Germany
[g] Department of Medical Biochemistry and Cell Biology at Institute of Biomedicine, Sahlgrenska Academy, The University of Gothenburg, Sweden
[h] Cell Growth, Tissue Repair and Regeneration (CRRET), UPEC EA 4397/ERL CNRS 9215, Université Paris Est Créteil, Université Paris Est, Créteil, France

ARTICLE INFO

Keywords:
Critical limb ischemia
Glycosylation
Elastin
Hydrogel
Angiogenesis

ABSTRACT

Critical limb ischemia (CLI) is characterized by the impairment of microcirculation, necrosis and inflammation of the muscular tissue. Although the role of glycans in mediating inflammation has been reported, changes in the glycosylation following muscle ischemia remains poorly understood.

Here, a murine CLI model was used to show the increase of high mannose, α-(2, 6)-sialic acid and the decrease of hybrid and bisected N-glycans as glycosylation associated with the ischemic environment. Using this model, the efficacy of an elastin-like recombinamers (ELR) hydrogel was assessed. The hydrogel modulates key angiogenic signaling pathways, resulting in capillary formation, and ECM remodeling. Arterioles formation, reduction of fibrosis and anti-inflammatory macrophage polarization wa also induced by the hydrogel administration. Modulation of glycosylation was observed, suggesting, in particular, a role for mannosylation and sialylation in the mediation of tissue repair. Our study elucidates the angiogenic potential of the ELR hydrogel for CLI applications and identifies glycosylation alterations as potential new therapeutic targets.

1. Introduction

Critical limb ischemia (CLI) is a manifestation of severe peripheral artery disease (PAD). CLI arises due to occlusion of vital blood vessels in the lower extremities. Each year, around 500–1000 new cases of CLI are diagnosed per million in the European and North American populations [1]. Angioplasty or surgical bypasses are the current gold standard treatments [2]. However, besides poor survival rates, prognosis of limb preservation is poor, particularly in patients with no-option CLI, where rates of major amputation within 6 months have been reported to range from 10% to 40%. Therefore, new therapies for this condition are urgently required.

In the interest of designing new therapies, several important considerations are necessary. One is to adopt a preclinical model that would closely mimic the circulation occlusion occurring in CLI patients. In our previous study it was demonstrated that the double ligation of femoral artery procedure was able to induce a robust ischemia in the BALB/c immunocompromised mouse [3]. Since the use of the wildtype mouse is more physiologically relevant, in this study, the double ligation procedure was used in the C57BL/6 wildtype mouse.

Another important consideration in developing a new therapeutic is to identify molecular alterations as biomarkers of the pathological condition. Recently, evidence of the role of glycosylation in mediating pathological events associated with ischemia has emerged, such as injury-response angiogenesis and inflammation [4–6]. Specific glycosylation of the angiogenic receptors can influence the trigger of

* Corresponding author. CÚRAM SFI Research Centre for Medical Devices, National University of Ireland Galway, Ireland.
E-mail address: abhay.pandit@nuigalway.ie (A. Pandit).

https://doi.org/10.1016/j.biomaterials.2020.120641
Received 14 August 2020; Received in revised form 24 December 2020; Accepted 29 December 2020
Available online 4 January 2021

angiogenic pathways. For example, α-(2,6)-sialylation of the vascular endothelial growth factor receptors (VEGFR) seems to be crucial in mediating their binding with the VEGFA ligand [7], and the binding of galectin-1 has also been shown as one of the mechanisms of tumor-associated angiogenesis [8]. In inflammation, glycosylation mediates the recruitment cascades of leukocytes by modulating selectin interactions both on endothelium and inflammatory cells [9]. However, the overall change in glycosylation in response to the ischemic injury is not known nor its potential role in injury and tissue repair.

Extracellular matrix (ECM)-based hydrogels have been used to deliver stems cells, growth factors, and genes and have shown promise in restoring a healthy microenvironment in ischemic models [10,11]. Such platforms can also be used for the delivery of growth factors or cells and they can be functionalized with molecules of interest [10–13]. Elastin is one of the essential components of ECM found in several tissues including arteries and skeletal muscle where it provides mechanical support, elasticity and resilience, and elastin peptide/fragments are involved in cell-signaling events such as proliferation and in inducing angiogenesis [13,14]. All of these properties make elastin an attractive candidate for biomaterials scaffolds for medical applications. However, the natural insolubility of elastin and its limited availability from animal sources has restricted its use for bio-engineering constructs. These limitations are avoided with the development of the elastin-like recombinamers (ELRs).

ELRs are a family of genetically engineered polypeptides whose sequence is based on native tropoelastin, specifically on the repeat of the pentapeptide (VPGXG), where X can be any amino acid except proline [15]. ELRs retain properties similar to those of natural elastin such as elasticity, low thrombogenicity, cytocompatibility self-assembly and thermoresponsive behavior. ELRs can also be functionalized by inserting specific bioactive sequences [16–19]. Recently, ELRs have been used in hydrogel/constructs that have shown their ability to stimulate angiogenesis *in vitro* and *in vivo* [19,20]. Here, two different ELRs constituted in a hydrogel using a click chemistry approach were used. Both ELRs present the (VPGXG)n backbone differ with the presence of two different bioactive sequences: 1) HE5-cyclooctyne carrying the matrix metallo-proteases (MMPs) binding site and, 2) HRGD-azide with an RGD sequence, binding site for integrins.

The hypothesis of the study presented here is that the double ligation of femoral artery CLI model can be used to identify glycosylation modifications that can serve as a biomarker of ischemia (Phase I, Fig. 1). Secondly, it was hypothesized that ELR-based hydrogel treatment would promote the formation of new blood vessels, ECM remodeling *in vivo* accompanied by modulation of the glycosylation and the protein regulatory pathways in the ischemic tissues (Phase II, Fig. 1).

2. Results and discussion

2.1. Phase I the ischemic muscle has unique glycosylation

Despite their well-recognized biological roles, glycans are still the least understood class of biomolecules in the context of ischemia. Currently, the knowledge of human or mouse muscle glycosylation is based on the lectin histochemistry of tissue and gene expression analysis [21]. Although studies focusing on glycosylation changes following ischemic insults on various visceral organs such as the heart and brain have been presented [22,23], there is a paucity of reports on the impact of ischemia on skeletal muscle glycosylation. Only recently, the loss of endothelial hyaluronic acid was described to impaired microvascular perfusion and endothelial stability in a murine CLI model [24]. This study sets out to address a gap in the current understanding of the influence of ischemic insult on the glycosylation in this tissue. Liquid chromatography electrospray ionization mass spectrometry (LC-ESI-MS/MS) analysis was used to characterize the effect of ischemia on N-glycome structures. In total, 51 N-linked glycan structures were identified. For comparison, individual glycan structures were quantified relative to the total content by integration of the extracted ion chromatogram peak area and expressed as a relative intensity percentage (%)

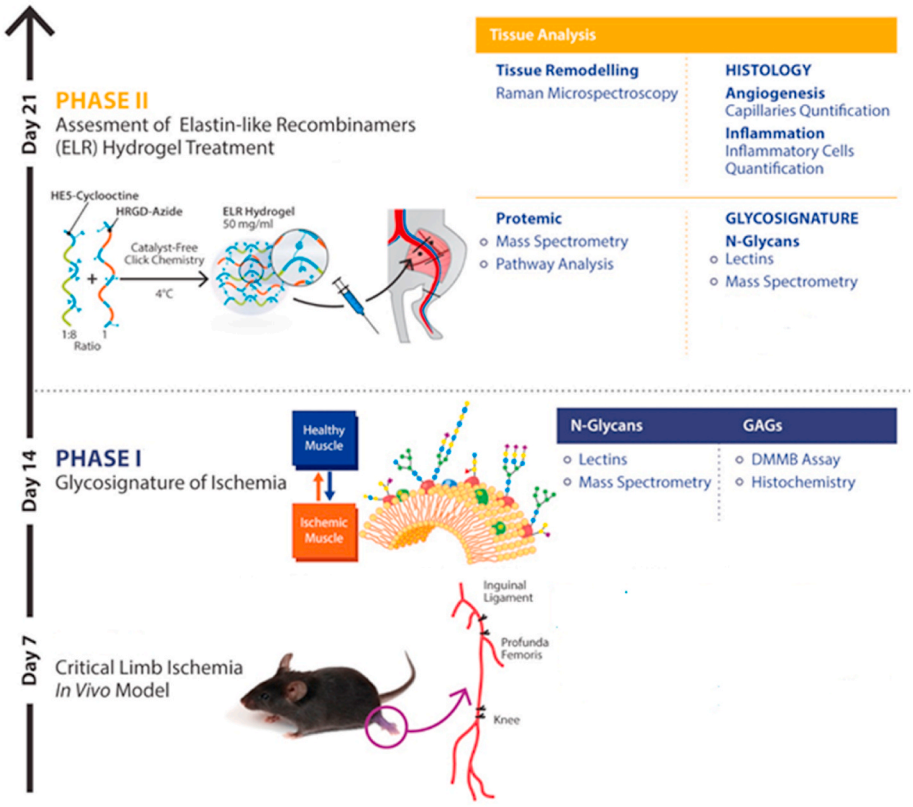

Fig. 1. Schematic representation of the experimental design. The study was designed as follows: phase I, phase II, characterization of the glycosylation of the CLI model; phase III, therapeutic efficacy of implanted ELR hydrogel following CLI injury. The analysis of all phases was carried out at 7, 14 and 21 days after the induction of ischemia. Phase I, double ligation of femoral artery as an ischemia model was adopted in the wildtype mouse. Ischemia was induced in the left limb of C57BL/6 mice by ligating the femoral artery, performing two occlusions, one before the *profunda femoris* collateral and the other one before the popliteal artery (Day 0). The glycosylation of the healthy hindlimb was compared with t that of the ischemic hindlimb. Specifically, N-glycans were examined using lectin histochemistry and LC-ESI-MS while GAG content was quantified by DMMB assay and immunohistochemistry. Phase II, The ELRs HE5-cyclooctyne and HRGD-azide solutions are mixed together in a ratio of 1.8:1 respectively for a final concentration of 50 mg/ml at 4 °C. The hydrogel solution (100 μl) was injected at the site of the first ligation at day 0. PBS was injected as control. Tissue remodeling and the angiogenic response were respectively analyzed by Raman microspectroscopy and stereological quantification of capillaries. The inflammatory response was assessed by stereological quantification of infiltrating inflammatory cells. The proteomic was analyzed by mass spectrometry and ingenuity pathway analysis. Lectin microarray and LC-ESI-MS/MS were adopted to examine the N-glycosylation response.

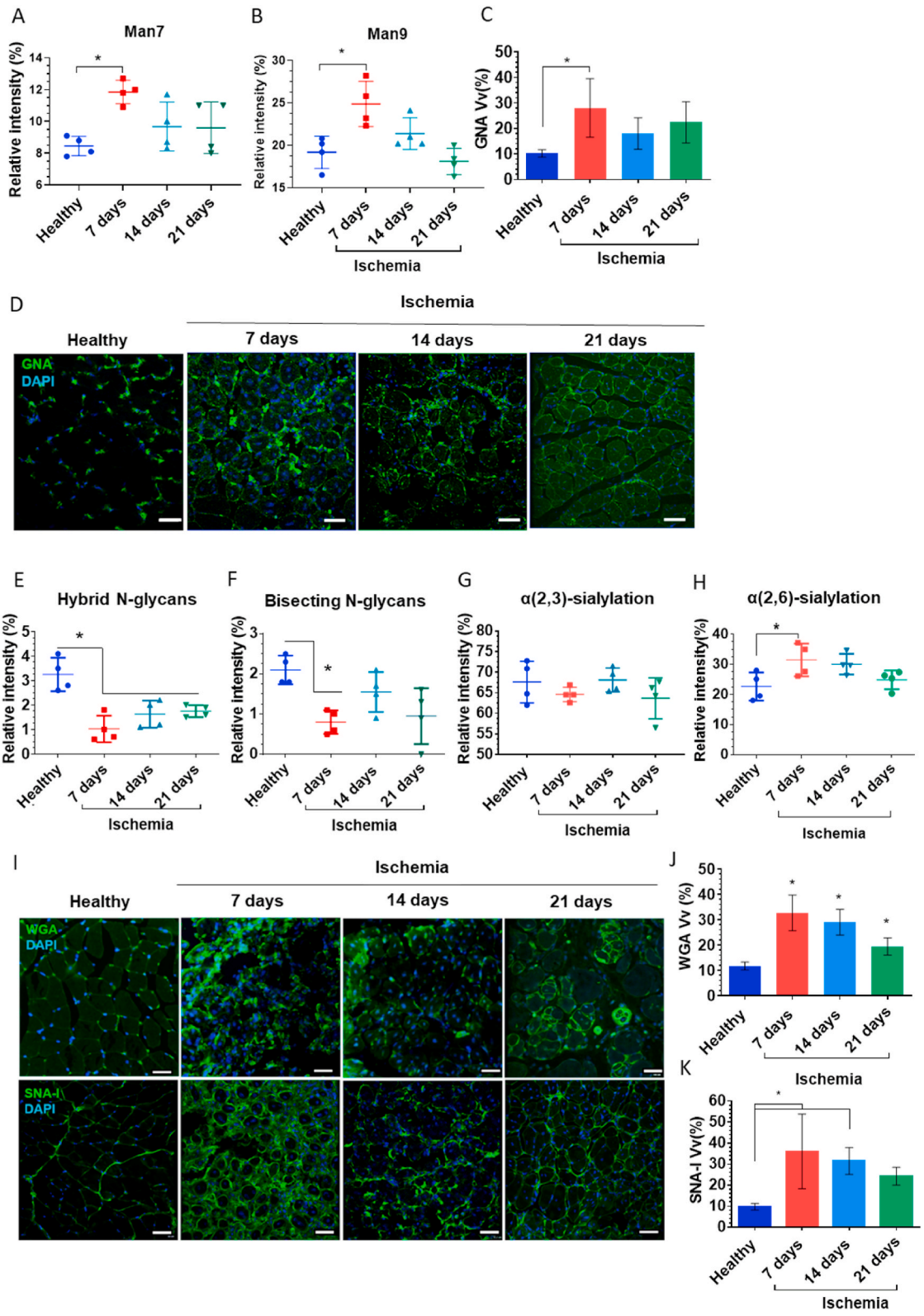

Fig. 2. N-glycosylation modifications after ischemia in the CLI model. Relative intensity percentage of A) the high mannose species, Man7 and B) Man9 by LC-ESI-MS/MS (n = 4) and C) Quantification of GNA signal expressed as volume fraction % (Vv%) (n = 6). D) GNA lectin histochemistry of healthy and of ischemic muscle tissues at post-operative days: 7, 14 and 21. Relative intensity of E) Hybrid N-glycans, F) bisected N-glycans, G) α-(2, 3)- sialylation, H) α-(2, 6)- sialylation by LC-ESI-MS/MS (n = 4). I) WGA, SNA-I and histochemistry of healthy and of ischemic muscle tissues at post-operative days: 7, 14 and 21. Quantification of the signals is expressed as volume fraction % of J) WGA K) SNA-I and lectins (n = 6). WGA that binds GlcNAc, SNA-I lectin binds α-(2, 6)-sialic acid and GNA lectin that binds to α-(1, 3)-mannose (scale bar = 50 μm, 20X magnification). Data are expressed as mean and standard deviation and significance between the groups was accepted for *$p < 0.05$, by One-way ANOVA.

(Fig. 2). To determine the baseline of the N-glycosylation context in physiological conditions, the composition of the healthy N-glycome was assessed (Fig. S1). Ischemia was successfully induced (using) the double ligation of femoral artery procedure (Fig. S2) and the healthy muscles were compared with ischemic ones at days 7, 14 and 21.

2.1.1. Ischemia promotes mannosylation in skeletal muscles

As depicted in Fig. 2A–D, the ischemia was found to affect the quantity of high mannose structures. In particular, the relative abundance of Man7 at day 7 (11.3 ± 0.74%) was significantly higher than that observed in the healthy samples (8.45 ± 0.6%) (Fig. 2A). The abundance of Man9 was also significantly higher in the ischemic samples (24.8 ± 2%) at day 7 than that of the controls (19 ± 1.9%), and still higher but not significantly higher at 14 days (21.3 ± 1.3%) (Fig. 2B). This relative increase of high mannose structures was also reflected in an absolute increase within the tissue using the lectin *Galanthus Nivalis* agglutinin (GNA), that binds to α-(1,3)-linked mannose. At 7 days after ischemia, a significant increase of GNA binding was observed (17.81 ± 11.5%) while at the other time points the same trend was still observed, although this was not significant (Fig. 2C and D). The GNA binding seems to be due to the presence of inflammatory cells and was also significantly increased in ischemia. The increase in expression of high mannose structure might be associated with the acute inflammatory response as protein high-mannosylation is a phenomenon that has a mediating role in inflammation [25].

2.1.2. Ischemia reduces hybrid and bisecting N-glycans content

Upon analysis of the response of hybrid type N-glycans to ischemic insults, 6 structures were detected by LC-MS. The relative intensity of hybrid N-glycans was significantly lower in the ischemic samples (1.0 ± 0.54% for day 7, 1.6 ± 0.55% for day 14 and 1.8 ± 0.23% for day 21) than that in the healthy control (3.2 ± 0.68%) (Fig. 2E). Three bisecting N-glycans were detected and the relative quantities of these were low. In comparison with healthy control (2.1 ± 0.35%), bisecting N-glycan in the ischemic tissue at day 7 (0.8 ± 0.29%) decreased significantly (Fig. 2F). The decrease of hybrid structures and bisecting N-glycans was observed in the acute phase of ischemia, which is dominated by inflammation. Pro-inflammatory stimuli such as cytokines affect glycosylation of the endothelium during inflammation [26], suggesting that the reduction of those structures may be due to this phenomenon. Furthermore, the functional role of the bisecting GlcNAc in down-regulated integrin-mediated cell motility is known [27]. This evidence suggests that the decreased expression of bisecting GlcNAc might be associated with an increase in the cell motility of inflammatory cells in the acute inflammatory phase.

2.1.3. Ischemia differentially regulates sialylation

A difference in the type of sialylation was detected in the ischemic samples from that of the healthy. A trend of increase of α-(2, 3)-linked sialyation was observed in the ischemic samples at 7 days (64.6 ± 1.6%) in comparison with healthy, even if not significant (Fig. 2G).

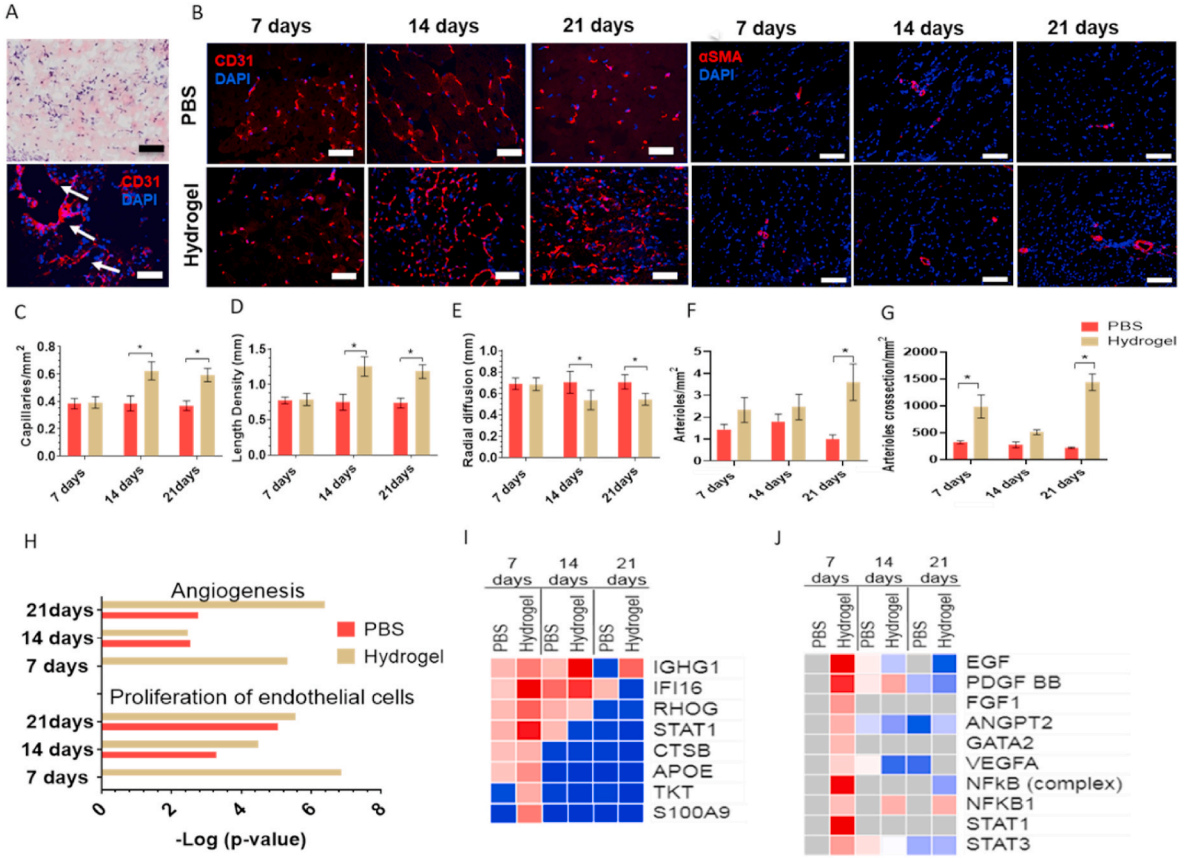

Fig. 3. Effect of the ELR hydrogel on angiogenesis. A) Infiltration of capillaries inside the hydrogel at 7 days after ischemia showed with H&E and CD31 staining (red) (20X), scale bar = 100 μm. B) Immunohistochemical CD31 (Red) staining for blood vessels and αSMA for arterioles of the muscle tissues from the ischemic control (PBS) and ELR hydrogel-treated tissue at days 7, 14 and 21 (20X magnification Scale bar = 20 μm). C) Capillary density, D) Length density and E) Radial diffusion stereological quantification. F) Arterioles density and G) arterioles area cross section quantification. H-J) Ingenuity pathway analysis (IPA) analysis of the proteomic data from protein extracts from the injured tissue and the hydrogel-treated at days 7, 14, 21 H) IPA identified biological function expressed as enrichment score (-log p-value) associated to angiogenesis and. I) Heatmap of fold change of the proteins the enriched biological function network. J) Heatmap of the top upstream regulators involved in the angiogenic process expressed as Z. Values are expressed as mean and SD (n = 6). Data are expressed as mean and SD and significance between the groups was accepted for *$p < 0.05$, by two-way ANOVA. (For interpretation of the references to colour in this figure legend, the reader is referred to the Web version of this article.)

Furthermore, a significant increase of the α-(2, 6)-linked sialylation was observed at 7 (31.5 ± 5.4%) ($p < 0.05$) and 14 days compared to the healthy (22 ± 6.5%) (Fig. 2H). This differential sialylation was also observed with *Wheat Germ* agglutinin (WGA) and *Sambucus Nigra* agglutinin (SNA-I) lectins. WGA binds to sialic acid regardless of linkage and N-Acetylglucosamine (GlcNAc) while SNA-I lectin binds to α-(2, 6)-linked sialic acid (Fig. 2I–K). In ischemic tissue at days 7 and 14, significantly higher binding intensities of WGA and SNA-I were observed over those in the healthy tissue (Fig. 2I–K). The volume fraction (Vv) % increase of WGA binding was 21 ± 7%, 17 ± 5%, 8 ± 3.3% respectively for days 7, 14 and 21. At day 21, WGA binding was more intense around the regenerating central nucleated fibers (CNFs) (Fig. 3I and J) SNA-I binding also increased significantly after days 7 and 14, respectively, to 26 ± 17% and 22 ± 6.4% (Fig. 3I, K). At day 21, there was no significant difference between the healthy and the ischemic tissue. WGA and SNA-I binding was associated with the inflammatory infiltrations. Hence, the relative quantity of α-(2–6)-linked sialic acid observed by LC-MS appears to reflect the absolute increase in the tissue, paralleling both the WGA and SNA-1 staining. Together, this indicates an increase of α-(2–6)-linked sialylation in ischemia.

α-(2, 3)-linked sialylation was decreased while α-(2, 6)- sialylation was increased, especially in the acute phase of ischemia (7 days). This suggests that ischemia influences the balance between α-(2, 3)- sialylation and α-(2, 6)- sialylation. Ischemia may alter the expression or intracellular distribution of the respective sialyltransferases ST3-Gal1 and ST6-Gal1. Furthermore, a depletion of α-(2,3)-sialylated glycans was observed in murine ischemic skeletal muscle fibers with lectin histochemistry [28]. The increase in α-(2, 6)-sialylated species was also observed at days 7 and 14, with the increased binding of SNA-I. SNA-I binding was associated with the inflammatory infiltrations. Also, the increase of WGA binding was associated with the inflammatory cells. Taken together, this evidence suggests that the decrease of α-(2, 3)-sialylation occurs on the fibers sarcolemma while the increase of α-(2, 6)- sialylation may be due to inflammatory cells. This increase may also indicate an interaction of leukocytes with selectins, well-known to be key players in inflammation, via sialic acid binding.

2.1.4. Chondroitin sulfate (CS) and heparan sulfate (HS) content in response to ischemia

To investigate the impact of ischemia on the muscle on glycosaminoglycans (GAG) content, enzymatic digestion, DMMB assay and immunohistochemistry with CS and HS specific antibodies were used (Methods S3). No significant difference in the total amount of GAG was observed in the healthy (0.2 ± 0.12 μ) and in the ischemic muscle after 7 (0.18 ± 0.06 μg), 14 (0.19 ± 0.07 μg) and 21(0.20 ± 0.07 μg) days (Fig. S4A). In the ischemic tissue at days 7, 14, and 21, the CS% percentage was 70 ± 19.4, 78.4 ± 12.31 and 77 ± 13.7, respectively, which was not significant when compared with the healthy tissue (71 ± 21.2%) (Fig. S4A). This result was confirmed with antibody staining for CS and HS in the skeletal muscle (Fig. S4C). These results indicate that the ischemic condition does not have an impact on either total quantity of GAGs or on relative composition. Recently, modifications of HS and CS structure (sulphation pattern) were observed in a rat model of CLI that was correlated with the progression of muscle regeneration [29]. Furthermore, the 6-O sulphation of syndecan-2 has recently been demonstrated to be crucial in regulating the crosstalk with VEGFR2 that mediates neovascularization in a murine model of CLI [30]. This suggests that the sulphation of HS and CS probably has a role in mediating the ischemic events and might be further investigated in this model.

2.2. ELR hydrogel induces capillaries and arterioles formation in the CLI model

2.2.1. ELR hydrogel has a pro-angiogenic effect in the ischemic tissue

2.2.1.1. Increase of capillaries in the hydrogel-treated tissue. The clinical success of any regenerative therapeutic strategy is premised on the revascularization and subsequent reperfusion of the newly formed vessels. Providing ECM components is a strategy to mimic the physiological cell niche and instruct the cells to activate proliferation and regeneration programs [31].

To evaluate the extent of blood vessel formation induced by the hydrogel, CD31 antibody was used as a capillary endothelial cell marker and the stereological parameters of capillary, length density and radial diffusion were determined. Fig. 3A shows the hydrogel seen in the ischemic tissue after 7 days (H&E) and the presence of capillaries within it (CD31). Fig. 3B shows CD31 staining in all the conditions.

At day 7, no significant difference in the capillary density between the ELR hydrogel treatment (0.39 ± 0.04) and the PBS control (0.38 ± 0.03) was observed. However, after 14 and 21 days, capillary density and length density significantly increased in the hydrogel-treated muscles (Fig. 3C and D). At day 14, a significant increase (63%) of capillary density in the hydrogel group (0.62 ± 0.026) over that of the PBS groups (0.38 ± 0.05) was observed. Furthermore, at this time point, the length density also increased in the ELR hydrogel-treated (1.2 ± 0.13) over that in the control group (0.74 ± 0.11) (Fig. 3D). After 21 days, the increase of capillary density was 63% in the hydrogel-treated group (0.59 ± 0.04) compared to the non-treated muscle (0.36 ± 0.03). At the same time point, the length density was also significantly increased in the hydrogel-treated tissue (1.18 ± 0.09) in comparison with the control group (0.73 ± 0.09) (Fig. 3D). Furthermore, a significantly lower radial diffusion (Fig. 3E) was observed in ELR hydrogel groups (0.53 ± 0.03 for day 14, 0.54 ± 0.02 for day 21) than that of controls (0.70 ± 0.04 for day 14, 0.70 ± 0.04 for day 21), which is a measure of the distance between the capillaries.

2.2.1.2. Increase of arterioles density and arterioles cross section. To measure if the hydrogel was able to stimulate arteriogenesis, αSMA antibody was used as an arterioles cell marker and the stereological parameters of density and cross section area were determined. Fig. 3B shows αSMA staining in all the conditions.

At days 7 and 14 no significant difference in the arterioles density between the ELR hydrogel treatment (1.45 ± 0.39 at day 7, 1.8 ± 0.6 at day 14) and the PBS control (2.33 ± 0.98) at day 7, 2.46 ± 1 at day 14) was observed. However, after 21 days, the arterioles density significantly increased in the hydrogel-treated muscles (3.6 ± 1.4) over that in the control group (1 ± 0.34) (Fig. 3F).

At day 7, a significant increase of arterioles cross section in the hydrogel group (990 ± 377) over that of the PBS groups (325 ± 46) was observed. While at day 14, no significant difference was observed in the groups (277 ± 92 for the PBS and 510 ± 79 for the hydrogel), a remarkable increase of the cross section area of the arterioles was seen in the hydrogel treated group (1439 ± 265) over to that of the PBS control (220.34 ± 22) (Fig. 3G). These results suggest that the ELR hydrogel influences arteriogenesis both by inducing the formation of collateral arteries, but also by remodeling of existing arterial vessels to a larger diameter.

To measure whether the hydrogel improves blood perfusion in the ischemic leg, laser Doppler imaging was recorded pre-operatively and immediately post-operatively, at 7, 14, and 21 days after the induction of ischemia (Fig. S5). Specifically, at day 7, no significant difference was observed between the perfusion ratio in the control group (PBS) (23 ± 12%) and in the hydrogel-treated (21 ± 0.12%), while at 14 days the ELR hydrogel group had a perfusion ratio of 43 ± 13% in comparison to 43 ± 11% of the ischemic control. At day 21, the perfusion ratio was 53

± 26% in the ELR hydrogel group while in the ischemic control it was 45 ± 15%. Here we showed that the ELR hydrogel treatment remarkably promoted an increase in the formation of new capillaries and arterioles in muscle tissues. However, there was no corresponding increase in perfusion in the skeletal muscles when evaluated by laser Doppler imaging. This apparent disparity could be a consequence of differences in sensitivity between histology and the Doppler imaging methods. Therefore, the ability of the ELR hydrogel to target the proteome signature underlying angiogenesis was investigated.

2.2.1.3. Enrichment and activation of pathways involved in angiogenesis. To determine the proteins and the biological pathways involved in the capillary outgrowth observed in the hydrogel-treated groups, protein expression was analyzed by 4-plex TMT protein tagging and subsequent liquid chromatography coupled to tandem mass spectrometry (LC-MS/MS). Protein-level estimates of expression and ratios between the different conditions were normalized to the healthy tissue as reference. The ratio is expressed as –log2 fold change. The maximum fold change for the protein group is at least ±1.5. For Ingenuity Pathway Analysis (IPA), the −log (p value) threshold was set at 1.3 to determine dysregulated biological function from the data set of the differentially expressed proteins. It was found that the biological functions such as angiogenesis and proliferation of endothelial cells were highly enriched in the ELR hydrogel-treated group especially at days 7 and 21 (Fig. 3H).

Fig. 3I illustrates the fold change of the proteins associated with the angiogenesis network. Several of these proteins present a higher fold change in the hydrogel-treated groups. Immunoglobulin heavy constant gamma 1 (IGHG1) particularly exhibited a higher fold-change in the hydrogel-treated group than that of the PBS control at days 7, 14 and 21. Interferon-inducible protein 16 (IFI16) was upregulated in the hydrogel-treated group compared to the PBS control at days 7 and 14. Other proteins in the angiogenic network presented a higher fold change in the hydrogel-treated group at day seven: Ras homology GTPase (RHOG), signal transducer and activator of transcription-1 (STAT1), Cathepsin B (CTPB), Apolipoprotein E (APOE), transketolase (TKT), S100 calcium-binding protein A9 (S100A9) (Fig. 3I). This evidence suggests the involvement of these proteins in the formation of new capillaries observed histologically. In particular, Rho GTPases mediate junctional remodeling and endothelial cells migration during angiogenesis [32]. The ELR hydrogel presents RGD (Arg-Gly-Asp) integrin binding motifs that are able to activate Rho GTPases pathway, which is involved in the cytoskeleton movement [33] and has here been found to be upregulated in the hydrogel-treated group at day 7. ELR presenting the RGD sequence have been shown to recruit endothelial cells in *in vitro* experiments and to promote their proliferation in comparison with the unmodified ELRs control [20]. ELR presenting systems have been shown to induce capillary formation in different *in vivo* models such as a subcutaneous mouse model [19] and an ectopic bone formation model in rats [20]. This evidence suggests that the RGD sequence is crucial in the ELR hydrogel's ability to recruit endothelial cells and to activate a synergy of pro-angiogenic programs. Infiltration of capillaries was observed inside the hydrogel at day 7, suggesting that the recruitment of endothelial cells results in the formation of sprouting capillaries within the hydrogel network. It is also important to note the upregulation of the matrix metalloproteinase (MMP) Cathepsin B (CTPB). The hydrogel presents an MMPs-sensitive site that attracts MMPs that mediate its degradation and therefore produce elastin-like fragments. Considering that Elastin peptides are known for their proangiogenic potential, these data suggest that MMPs-sensitive site can contribute to the angiogenic process not only by promoting the infiltration of the endothelials cells but also by producing elastin-like peptide fragments that can exhibit an angiogenic effect [34]. Further studies on the characterization of these peptides and their action in presence of endothelial cells could confirm this mechanistic hypothesis. In our previous study [10] where an elastin-like polypeptide (ELP) lacking both a cell adhesion sequence and an MMP degradation site, was tested as a gene delivery system in a mouse model of CLI, it was observed that elastin alone was not able to induce angiogenesis. Taken together, all these observations suggest that the angiogenic potential of this ELR hydrogel relies on the presence of the RGD and the MMP sequence, and this makes it attractive for biomaterial alone applications.

Furthermore, among the upstream regulators of the cellular functions, Epidermal growth factor (EGF), platelet-derived growth factor BB (PDGF-BB), fibroblast growth factor-1 (FGF1), Angiopoietin-2 (ANG-2), GATA-binding factor 2 (GATA2), Vascular Endothelial growth factor (VEGFA), nuclear factor kB (NF-kB), signal transducer and activator of transcription-1/3 (STAT1/3) were activated and upregulated in the hydrogel-treated tissue at day 7 compared with the injected PBS control (Fig. 3J). These upstream regulators are known to regulate angiogenesis pathways. The molecular network interaction activated by these upstream regulators is illustrated in Fig. S6. The synergy of proangiogenic growth factors activated pathways in mediating angiogenesis is well-known [35,36]. Blood vessel stability relies on the crosstalk of multiple signaling pathways in the endothelium and pericytes [35,36]. NF-kB and STAT1/3 are pathways involved in the process and are found upregulated with the ELR hydrogel treatment. VEGF can induce endothelial cell migration and proliferation by activating STAT1/3 signaling [37]. The interaction of VEGF and PDGF-BB has also been reported in the formation of stable capillaries: while VEGF promotes endothelial cell proliferation, PDGF-BB stabilizes blood vessels by recruiting pericytes [36]. FGF1 also can interact with VEGFA and control the secretion of PDGF-BB, contributing to the formation of stable vessels [38].

Taken together, these results indicate that the ELR hydrogel stimulates angiogenesis *in vivo* through a synergic action of pro-angiogenic pathways.

Raman microspectroscopy revealed differences in the extracellular matrix profile.

Since ECM matrix remodeling is a process that accompanies angiogenesis and arteriogenesis, the molecular profile of the ECM was evaluated with Raman microspectroscopy [39]. Raman analysis was performed on healthy, PBS control and ELR hydrogel-treated tissue sections. Overall, the Raman spectra showed differences between the healthy tissue and the PBS control (Fig. 4A–D). Additionally, the hydrogel-treated Raman spectra showed a degree of similarity to that obtained for healthy tissues (Fig. 4A, D, E, F). The resulting Raman spectra from healthy, ischemic tissues, and ELR hydrogel-treated muscle displayed the following vibrational peaks: 1343 and 1345 cm^{-1} assigned to CH_3, CH_2 wagging, 1450 and 1250 cm^{-1} to C–H, and C–H_2 deformations respectively and 1666 cm^{-1} (amide signals) (Fig. 4A, D). At day 7, peaks attributed to glycans (853 cm^{-1} - the glyosidic C–O–C bond) and to (891, 841 cm^{-1} – the saccharide band) have been observed to have a different intensity in the hydrogel different from that of the PBS injected (Fig. 4A). After 21 days, the average spectrum of the ischemic tissue also shows a high intensity in the 1666 cm^{-1} peak associated with the amide I compared to the healthy Fig. 4D). Raman spectra were compared with PCA, a multivariate analysis method, where spectral information is reduced to so-called PC scores and the variances are plotted in a PC loading spectrum. The multivariate analysis depicted three separated clusters for the healthy and the ischemic groups at days 7 and 21 (Fig. 4B), while overlapping clusters for the healthy and hydrogel-treated groups both at days 7 and 21 (Fig. 4E) were observed.

The difference between the distinct spectra populations (healthy versus ischemic at days 7, and 21 is depicted in the loading spectra (Fig. 4C). The loading spectra of PC-2 illustrates the Raman signals that vary predominantly in the band such as lipids C–C–N symmetric stretching (571 cm^{-1}), the C–O–C carbohydrate ring (878 cm^{-1}) (948 cm^{-1}), phospholipid structural changes (1130 cm^{-1}), and amide bands (1486, 1686 cm^{-1}).

The distribution of PC-3 and PC-2 score values showed the formation of three overlapping clusters of population between the healthy and the hydrogel-treated at days 7 and 21 (Fig. 4E). The spectra similarities

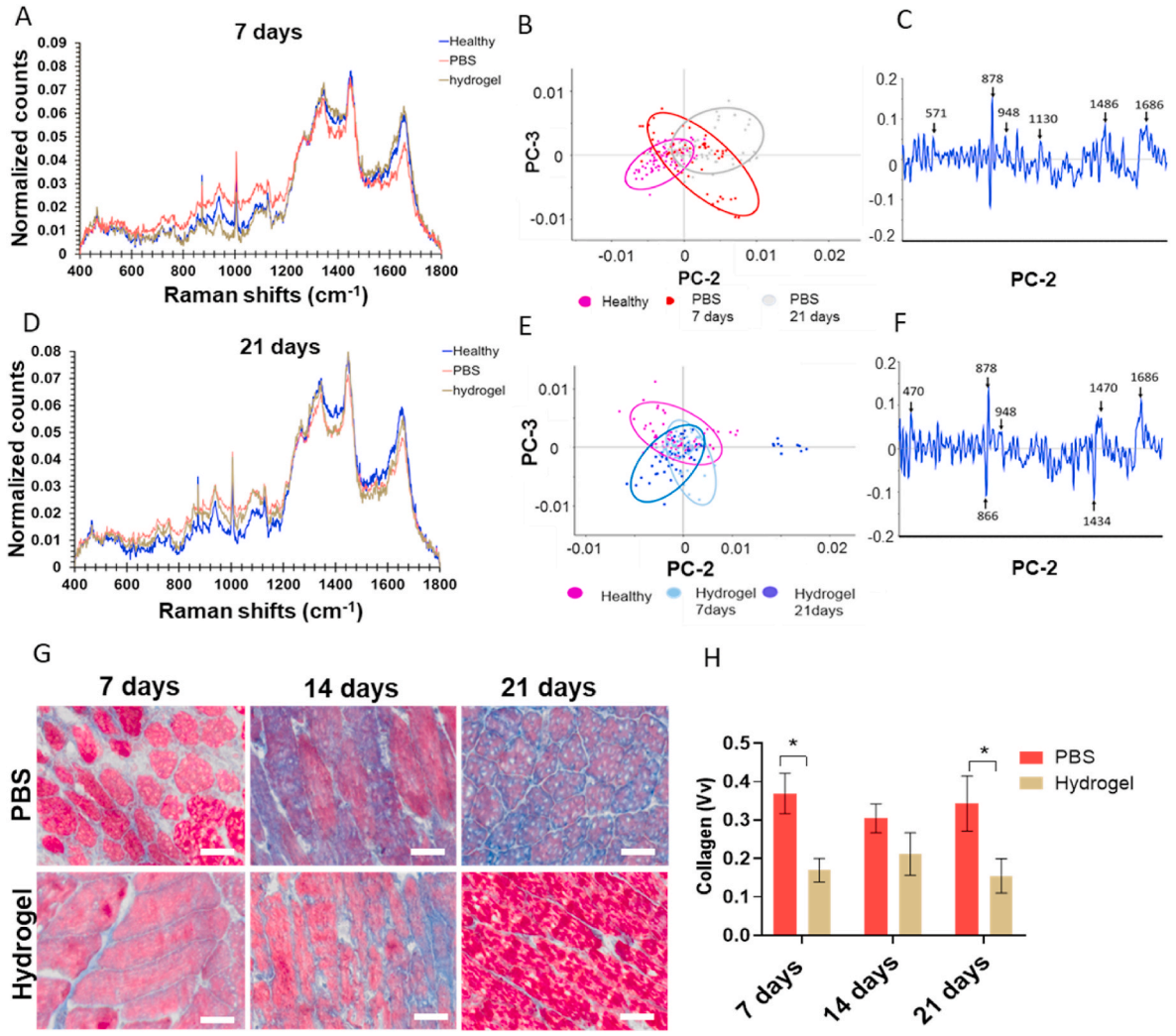

Fig. 4. Raman Microspetroscopy profile of the healthy tissue and collagen deposition, the ischemic control (PBS) and ELR hydrogel-treated. A) Average Raman spectra comparison of the ischemic control (PBS) and ELR hydrogel-treated tissue at day 7. B) Principal component analysis (PCA) and C) PC-2 loadings of the healthy and the injured control at days 7 and 21. D) Average Raman spectra comparison of the ischemic control (PBS) and ELR hydrogel-treated tissue at day 7. E) PCA, and F) PC-2 loadings of the healthy and the ELR hydrogel-treated tissue at days 7 and 21 (n = 3). G) Masson's trichrome staining (20x magnification, scale bar = 50 μm) and H) Volume fraction (Vv) quantification of collagen deposition (n = 3). Data are expressed as mean and SD and significance between the groups was accepted for *$p < 0.05$, by two-way ANOVA.

between the healthy and the ELR hydrogel-treated are depicted in the PC2 loading scores (Fig. 4F). The spectra were similar in the Raman peaks of the C–O–C carbohydrate ring (878 cm^{-1}) (948 cm^{-1}) (1434 cm^{-1}), C═N stretching (1470 cm^{-1}) amide I C═C stretching vibrations (1686 cm^{-1}). These results indicate that the hydrogel induces a remodeling of ECM components such as glycans and structural ECM proteins. ECM remodeling plays crucial roles in regulating of the angiogenic processes [40]. Specifically, the ECM can interact and/or store several pro-angiogenic growth factors and cytokines. The ECM remodeling can subsequently release the growth factors which favor the sprouting of endothelial cells [41]. These observation suggests a link between the ECM remodeling and the angiogenesis induced by the hydrogel.

2.3. The hydrogel reduces the deposition of collagen and the consequent fibrosis

Since the formation of uncontractile fibrotic scar (fibrosis) occurs after the ischemic injury and the Raman data indicated a possible remodeling of ECM components including collagen, Masson's trichrome was used and quantified to evaluate the effect on the hydrogel on fibrosis. It was observed that the hydrogel was able to reduce the collagen deposition at day 7 and 21 (Fig. 4G and H).

In particular, at day 7 the Vv fraction of collagen significantly decreased in the hydrogel treated tissue (0.17 ± 0.031) when compared to the control (0.369 ± 0.053). At day 14 a trend of collagen Vv reduction was still observed even though not significant (0.305 ± 0.038 for the PBS-treated and$\pm$ 0.212 for the hydrogel-treated). The reduction of the collagen volume fraction was still significant at day 21 in the hydrogel-treated group (0.155 ± 0.045) when compared to the PBS-treated (0.343 ± 0.072). This result is consistent with our recent study [41] where the ELR hydrogel reduced collagen deposition when implanted in the skeletal muscle in a rat model of volumetric muscle loss (VML).

2.4. ELR hydrogel modulates macrophages polarization towards anti-inflammatory phenotype

To determine whether the ELR hydrogel had an effect on the ischemic-induced inflammation, infiltrating inflammatory cells were stereologically quantified. No significant difference in the infiltration of inflammatory cells was observed in the ELR hydrogel-treated group or in

the PBS group at any of the time points (Fig. 5A and B). Immunostaining for CD68, a marker for activated macrophages, further confirmed the inflammation in the ELR hydrogel-treated compared to the control groups (Fig. 5A). The volume fraction was 0.73 ± 0.4 and 0.72 ± 0.37, respectively, for the ELR hydrogel and the control group at day 7, 1.1 ± 0.05 and 1.03 ± 0.30 at day 14 and 0.27 ± 0.22 and 0.23 ± 0.11 at day 21 (Fig. 5B).We next asked if the hydrogel could have a positive effect on macrophage polarization, as previously demonstrated [42]. For this purpose, the tissues were analyzed for CD163 a marker of M2 anti-inflammatory macrophages. Even though no significant difference was seen at days 7 and 14, a significant increase of the infiltration of CD163+ cells was observed in the hydrogel-treated tissue (13.067 ± 4.6) when compared with the ischemic control (6.46 ± 2.6) (Fig. 5C). This data suggests that ELR hydrogel able to modulate the macrophage response and facilitate the shift to anti-inflammatory M2 macrophages. This observation agrees with a previous study where ELRs were reported to induce macrophage polarization in skeletal muscle that was associated with lower collagen deposition [42]. Further studies will have to elucidate the mechanism of the immunomodulation mediated by the ELR hydrogel.

2.5. ELR hydrogel modulates mannosylation and sialylation

The role of glycans in the context of biomaterial-host response has long been underestimated. In our previous study [43], the role of GAGs in the angiogenesis induced by a collagen/IL-6 siRNA/eNOS pDNA system was elucidated in a subcutaneous rat model. In more recent study, N-glycans remodeling was observed along the angiogenic response evoked by a collagen MSCs 3D hydrogel in the same hindlimb ischemia model used in this study [44]. Since in this study it was found that ischemia induces dynamic changes in N-glycosylation, the efforts were focused on investigating the effect of the hydrogel treatment on N-glycosylation. To do so, overall N-glycosylation changes induced by the ELR hydrogel, protein extracts from healthy, the ischemic injured (PBS) and the ELR-treated samples were incubated with a lectin microarray (Table S6). Clustering analysis of the samples showed that lectin binding distinguished the glycosylation of the healthy, the ischemic controls, and the hydrogel-treated groups at 7, 14 and 21 days (Fig. 6A). There was a clear distinction between the profiles of the injured control at day 21 and all the other conditions, including the healthy, with a 15% similarity.

Differential binding of the samples with lectins that have affinity for sialic acid (WGA, MAA, SNA-I), terminal α-linked galactose (VRA, MOA) and mannose residues (Calsepa) was detected at every time point (Fig. 6A). There was a dramatic reduction in binding to MAA, which is specific for α-(2,3)-linked sialic acid, observed in both the ischemic control and the hydrogel-treated condition. This was in contrast to the healthy tissue which had intense binding to MAA. These results suggest that the ischemic environment results in a reduction in the expression of α-(2,3)-linked sialic acid. The hydrogel treatment does not appear to have an effect on MAA binding but it does seem to have an effect on SNA-I binding.

These observations were validated by investigating N-glycans using by LC-ESI-MS/MS. The analysis was carried out on total protein extracts from the healthy, injured and ELR hydrogel-treated samples (n = 5–8). In total, 76 selected N-glycans structures were identified and used for comparison. Overall, differences in the quantity of high mannose structures and sialylation were observed in the hydrogel-treated tissues when compared to the ischemic control and the healthy tissue (Fig. 6B–J). A significant reduction of the relative intensity of total high-mannose types has been observed in the ELR hydrogel-treated group (20 ± 4.8%) in comparison with the injured control (29.7 ± 6.4%) and the healthy (29.4 ± 5.3%) at day 7 (Fig. 6B). At day 14 also a significantly lower quantity of total high mannose type structures was found in the hydrogel-treated samples (21.4 ± 6.8%) in comparison with the healthy tissues (Fig. 6B). To determine whether the decrease of total mannose observed in the hydrogel-treated tissues was due to a particular structure, the relative intensity of each high-mannose type N-glycans (from Man_1-Glc_1Man_9) was calculated. The ratio of Man5/Man9 did not show a significant difference in any of the conditions (Fig. 6C). A decreased

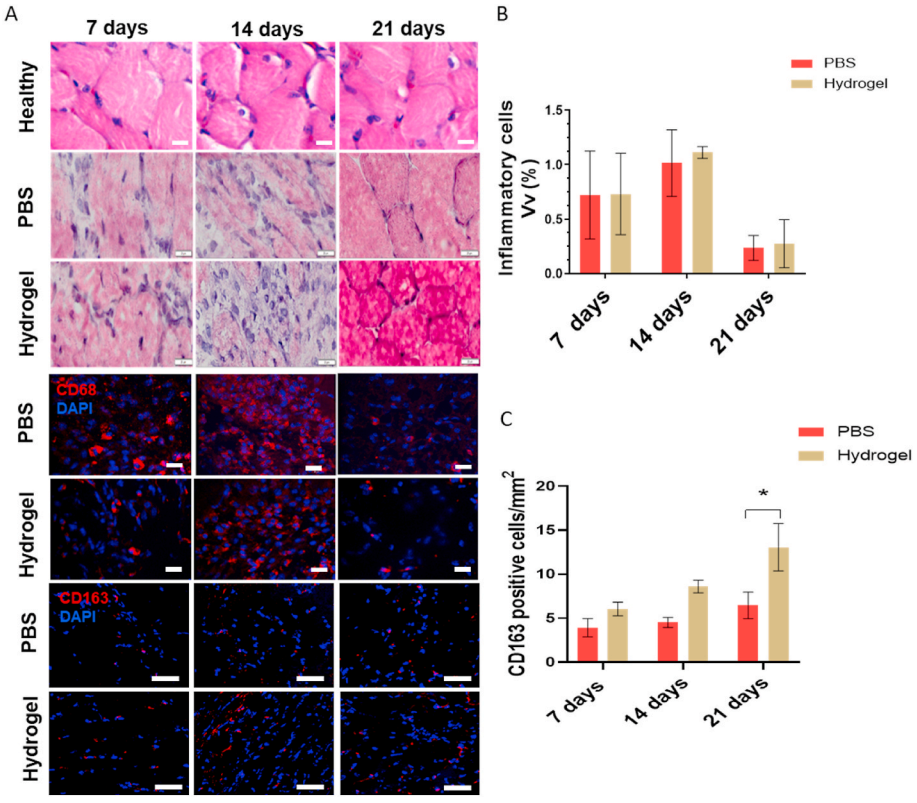

Fig. 5. Effect of the ELR hydrogel on Inflammation. A) H&E (40X magnification Scale bar = 20 μm), CD68 staining for macrophages and CD163 for anti-inflammatory macrophages staining of the muscle tissues from the ischemic control (PBS) and ELR hydrogel-treated tissue at days 7, 14 and 21 (40X magnification Scale bar = 20 μm). B) Inflammatory cell volume fraction (Vv%) (n = 6) and C) CD136 quantification of the ischemic control (PBS) and ELR hydrogel-treated tissue at days 7, 14 and 21. Values are expressed as mean and SD. Data are expressed as mean and SD and significance between the groups was accepted for *p < 0.05, by two-way ANOVA.

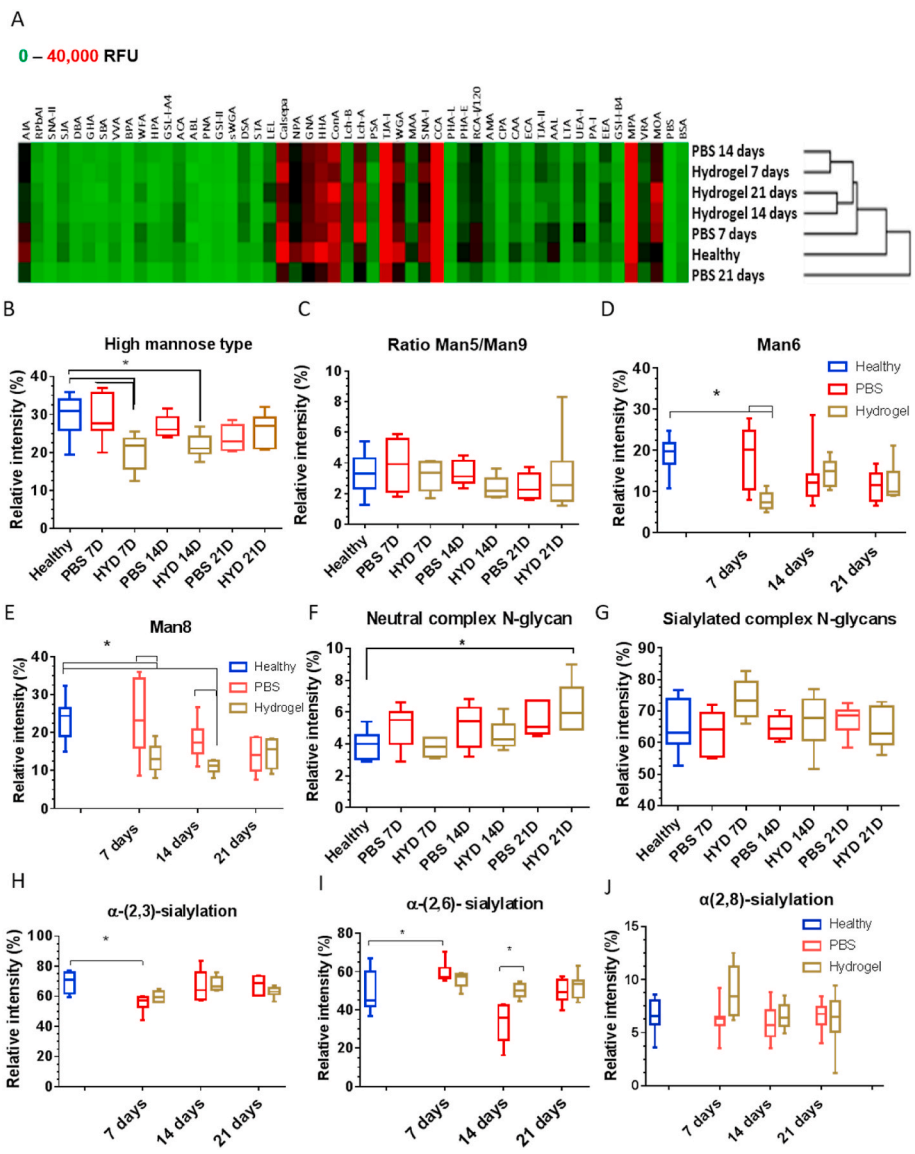

Fig. 6. The ELR hydrogel modulates mannosylation and sialylation in the ischemic muscle A) Lectins array analysis of the effect of the ELR hydrogel on glycosylation in the ischemic muscle. Clustering analysis was performed with total intensity mean normalisation, complete linkage, Euclidean distance and all 50 lectins printed were included. Relative intensity quantification of by LC-ESI-MS/MS of B) total high mannose N-glycans C) Man5/Man9 ratio D) Man6, E) Man8, F) Man8. Relative intensity of total F) neutral complex glycans, G) total sialylated N-glycans, H) α-(2, 3)- sialylation I) α-(2, 6)- sialylation and J) α-(2, 8)- sialylation. Data are expressed as mean and (SD) and significance between the groups (n = 5–8) was accepted for *p < 0.05, by two-way ANOVA.

level of Man6 and 8 was observed in the hydrogel-treated groups relative to the ischemic control and the healthy groups (Fig. 6D and E). In particular, Man6 was 11% decreased in the hydrogel-treated group at (7.4 ± 6.7%) at day 7 compared to the ischemic control (19 ± 7.4%) and the healthy tissues (19 ± 4.2%) (Fig. 5D). Furthermore, Man8 levels were found significantly reduced in the hydrogel-treated compared with the non-treated control at days 7 and 14 (Fig. 6E). Specifically, the reduction of Man8 was 10% and 6% respectively at days 7 and 14. These observations suggest that the reduction of total high mannose level observed in the hydrogel-treated samples might be due to a low level of Man6 and Man8 detected in the same groups. The literature points to the critical role of high mannose structures in the initiation and progression of inflammation [25].

In phase I, it was observed that ischemia prompts the level of high mannose species Man7 and Man9 in the acute inflammatory phase, while here it was found that the hydrogel treatment decreases the other two high mannose structures such as Man6 and Man8.

During inflammation, mannose residues are recognized and bound by C-type lectin receptors displayed by monocytes, macrophages and other inflammatory cells [45]. In particular, these C-type lectin receptors can recognise di-mannose and tri-mannose residues that are present in Man6 Man7, Man8 and Man9 that were found differentially modulated in this study. No significant differences in the inflammatory cell infiltration were observed in the hydrogel-treated groups at any of the time points. The decrease of high mannose structures observed in this study suggests a possible effect of the hydrogel in fine-attenuating inflammatory interactions. For example, the reduction of mannosylated glycans on the endothelial cell surface attenuates monocytes extravasation [46]. This hypothesis could be further investigated by deciphering mannose receptor-ligand interactions. An investigation of the sub-population of macrophages (anti-inflammatory or pro-inflammatory) could clarify a possible inflammation modulatory function of the hydrogel.

LC-ESI-MS/MS Fifty-two complex structures were identified, of which 45 were sialylated and 7 neutrals. A significant increase of neutral complex type N-glycans was observed in the hydrogel-treated group (6.2 ± 1.5%) at day 21 over that of the healthy control (3.9 ± 0.8%) (Fig. 6F). 52 complex N-glycans, including 45 sialylated and 7 neutral N-glycans. The sialylated N-glycans present were 60–80% of the total N-glycans (Fig. 6G). No significant differences were observed in the relative intensity of total sialylation across all the conditions (Fig. 6G), while differences in the relative intensity of different sialylation types were observed (Fig. 6H, J). The ischemic tissue at day 7 showed a significant reduction of α-(2, 3)-sialylation (56.67 ± 5.9%) in comparison with the

healthy (69 ± 6.8%) (Fig. 6H). At the same time point, the ELR hydrogel-treated showed an increasing trend of α-(2, 3)-sialylation even though this was not statistically different (59 ± 3.4%). No significant difference was detected between control and other conditions at days 14 and 21.

In regard to α-(2, 6)-sialylation, the ischemic tissue (59.6 ± 5.1%) at day 7 showed a significant increase over that of the healthy (49 ± 10%) (Fig. 6I). At day 14, the level of α-(2, 6)-sialylation increased in the hydrogel-treated group (55.3 ± 4.3) over that of the ischemic control (33.4 ± 10) (Fig. 6I). These results suggest that the hydrogel does not have an effect on α-(2, 3)-sialylation, but it does induce a significant increase of α-(2, 6)-sialylation at day 14. For α-(2, 8)-sialylation, no significant differences were found in any experimental group (Fig. 6J). Overall, the LC-ESI-MS/MS data suggest that the hydrogel is able to reduce the level of high mannose structures of total proteins at days 7 and 14. Furthermore, at day 14 the hydrogel seems to mediate an increase of α-(2, 6)-sialylation.

In this study, the increase of (2, 6)-sialylation in the hydrogel-treated group was concomitant with an increase of capillaries at day 14. Recently, a pro-angiogenic effect of α-(2, 6)-sialylation has emerged as it was reported to be a crucial determinant in mediating the binding of VEGF with its receptor-2[36]. Even though there was an increase in new capillaries at day 21 in the hydrogel-treated group, there was no corresponding increase in α-(2,6)-sialylation at this timepoint, suggesting that the hydrogel induced a transient increase of this type of sialylation. Unlike gene or protein expression, glycosylation is not template-driven but is regulated by many factors including the availability of nucleotide donors and the expression of enzymes [47,48]. Therefore, glycosylation modifications are more variable as they are more susceptible to stimuli caused by the environment. Hence, the transient increase of α-(2, 6)-sialylation can be considered as a molecular marker of a certain stage of the hydrogel-host response.

Further *in vitro* investigation with ELR-functionalized hydrogel and endothelial cells could reveal whether this α-(2,6)-sialylation-modulation is associated with the angiogenic process.

Taken together, these results suggest that the reduction of high mannose structures and the increase of α-(2, 6)-sialylation might be important post-translational modifications involved in the tissue repair process induced by the hydrogel. However, further studies are necessary to determine the mechanisms that are involved in the dynamic changes that occur in the N-glycome upon the hydrogel injection. A possible mechanism of the action of the hydrogel starts with the recruitment of endothelial cells. The hydrogel may activate the cross talk between the proangiogenic receptor's signaling pathways resulting in the cytoskeletal movement that is involved the angiogenic sprouting [31,49,50]. The degradation of hydrogel may favor the infiltration of the sprouting capillaries and also release elastin-like peptides with a pro angiogenic action. High mannose type structures and α-(2, 6)-sialylation on proteins may have a role in the hydrogel-induced remodeling. Fig. 7 summarizes the findings of this study.

3. Conclusions

Using a CLI murine model, it was demonstrated that ischemia altered the glycosylation of skeletal muscles, particularly that of mannosylation and sialylation. Decreased hybrid type and bisecting N-glycan expression was also observed. These findings indicate a role for glycosylation beyond inflammation in mediating the pathological and healing events during ischemic injury and may signal new opportunities in both diagnostic and therapeutic interventions. Moreover, using this model, it was demonstrated that the ELR hydrogel can not only induce the formation of new capillaries and arterioles but also can reduce fibrosis, and modulate macrophage polarization. The tissue healing was associated with remodeling of ECM components including glycosylation and protein expression. A possible mechanism involves the recruitment of the endothelial cells that surround and infiltrate the hydrogel and the activation of pro-angiogenic cytokine mediated pathways. Overall, our observations suggest that ELR hydrogel has a potential in the therapeutic application for the treatment of CLI.

4. Experimental section

4.1. CLI in vivo model

All animal procedures and treatments were approved by the ethics committee at the National University of Ireland, Galway. Animals were purchased from Charles River Laboratories and acclimated to the

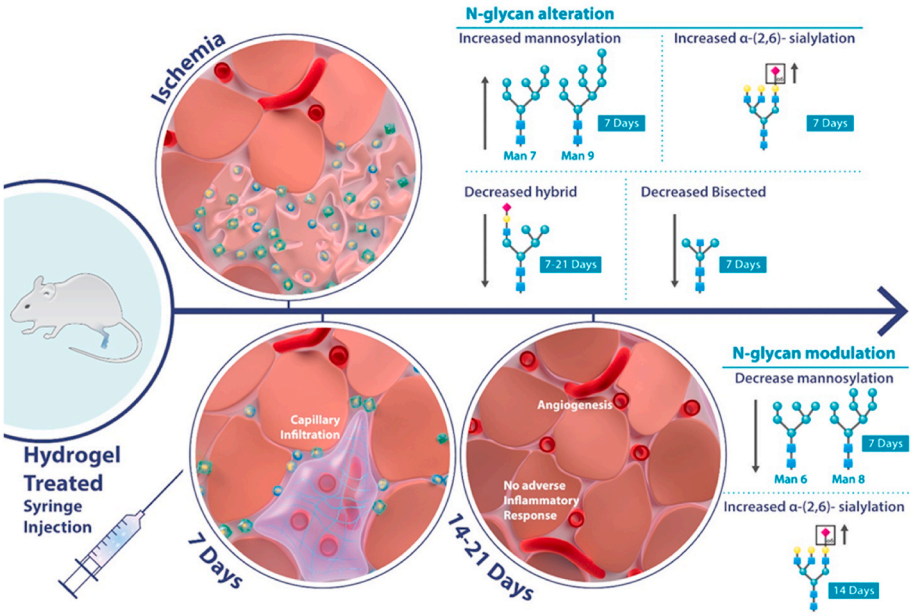

Fig. 7. Host response of the ELR hydrogel in the CLI model. The ELR hydrogel induced the formation of capillaries and ECM remodeling toward a healthy state. Decrease of mannosylation and increase of α-(2, 6)-sialylation were detected as post-translational modifications associated with the remodeling effect induced by the hydrogel.

vivarium for at least 14 days before the experiments were begun. Female C57BL/6NCrl mice, 10–12 weeks old, weighing 18–22 g, were anesthetized by the intraperitoneal injection of ketamine (80 mg/kg) and xylazine (10 mg/kg). The surgery and all the following analysis have been conducted in a blinded manner. Ischemia was induced in the left leg of the mouse by the double ligation of the femoral artery as previously described [3]. Briefly, the artery was ligated and cut in two locations, before the *profunda femoris* and before the saphenous-popliteal collaterals. For the characterization of the CLI model and the glycosylation analysis, sample sizes were n = 9–10 (healthy, ischemia 7 days, ischemia 14 days, ischemia 21 days). For the *in vivo* testing of ELR hydrogel, sample sizes were n = 11 for each group (PBS injected and ELRs treated with time points day 7, 14 and 21). The time points (7–21 days) have been optimized in our previous *in vivo* CLI studies [3,10,44] as they capture the acute phase of ischemia (7 days), an intermediate response phase (14 days) and the late tissue remodeling phase (21 days).

4.2. Functional analysis of blood perfusion, ambulation and necrosis

Laser-Doppler scanning was performed immediately pre- and post-operatively, and at days 7, 14 and 21 to monitor hind-limb perfusion. Perfusion changes were recorded and quantified from the plantar region of the foot using the moorLDI review V6.0 The recovery of blood flow was expressed as a ratio of ischemic left leg to non-ischemic right leg. The recovery of the ambulation capacity and the development of necrosis were semi-quantitatively determined using grading scales based on the gross observation of the operated foot. **Ambulatory scoring scale: 0** Flexing the toes to resist, traction on the tail similar to that on the non-operated foot, **1** Plantar flexion but not flexion of toes, **2** No dragging foot but no plantar flexion, **3** Dragging the foot. **Necrosis scoring scale*:* 0** Normal toes, **1** Mild redness or cyanosis of tips of toes/nails, **2** Cyanosis of toes and/or mild necrosis of toe/s (toe count), **3** Severe necrosis, **4** Auto-amputation of distal limb.

4.3. ELR hydrogel preparation and administration

The ELRs were designed, synthetized and provided by the BIOFORGE group at the University of Valladolid, Spain. The ELRs are composed by the repetition of the tropoelastin pentapeptide (VPGXG) n in which X is any amino acid except L-proline. In this study, two ELRs differing in the presence of two different bioactive sequences were adopted: 1) HE5-cyclooctyne carrying the matrix metallo-proteases (MMPs) binding site and 2) HRGD-azide with an HRGD sequence [46], binding site for integrins. A brief description of the ELR hydrogel characterization is presented in Material S7, Fig. S8 (Contessotto et al., under revision).

For the *in vivo* testing, the ELRs HE5-cyclooctyne and HRGD-azide were dissolved separately in cold phosphate buffered saline (PBS, pH 7.4) and mixed in a ratio of 1.8:1 respectively. The click chemistry reaction between the cyclooctyne and azide residues allows the hydrogel formation in a catalyst-free manner. After 10 min in ice, a total of 100 μl of the hydrogel was injected at the proximal artery ligation site after surgical induction (Day 0). Specifically, two injections were performed using a 100 ml syringe with a 27G needle: 50 μl of the hydrogel was injected in the quadriceps, and another 50 μl in the hamstring.

4.4. Histology

The animals were sacrificed and the skeletal muscles (gastrocnemius and quadriceps) were collected from the healthy, the not treated ischemic leg and the ELR hydrogel-treated leg at days 7, 14 and 21 after the induction of ischemia. Muscle biopsies were snapfrozen in optimal cutting temperature (OCT) compound (TISSUE-TEK®; Sakura Finetek USA. Inc.) with liquid nitrogen and cryopreserved at −80 °C for histology. Tissue sections (7 μm) were taken from four different depths at 50 μm intervals using a Leica CM1850 cryostat (Leica Microsystems, Germany) and collected on Superfrost™ Plus slides (Fisher Scientific, Dublin, Ireland) and stored at −20 °C until use.

H&E, masson thrichrome, immunohistochemistry, lectin histochemistry and Raman microspectroscopy measurements were performed on tissue sections. Three tissue sections from each mouse (n = 5–6) were used for histology, stereological quantifications and Raman measurements (n = 3).

4.5. Immunohistochemistry

For immunofluorescence, sections were washed three times in PBS and fixed in 4% PFA for 15 min. After three further washes in PBS, the tissue sections were blocked with 3% BSA for 2 h to avoid non-specific binding. Anti-mouse polyclonal primary antibody specific for CD31/PECAM-1 (1:200) (Abcam, Ireland) endothelial marker, primary mouse generated CD68 (1:200) (Abcam, Ireland) for macrophages, rabbit polyclonal to α-smooth muscle actin (α-SMA)(1:250) (ab5694, Abcam, UK) and rabbit polyclonal to CD163 (1:100) (ab87099, Abcam, UK). Secondary antibody labelled with AlexaFluor® 488 or AlexaFluor® 594, AlexaFluor® 546 (1:250) (Invitrogen, Ireland) was applied for 1 h at room temperature, followed by nuclear counter staining with DAPI (Life Technologies). The slides were washed in TBS-T before coverslip mounting with ProLong® Gold Antifade Mountant (Life Technologies). All slides were incubated at 4 °C in the dark for 24 h before imaging with an LSM710 confocal microscope (Carl Zeiss).

4.6. Lectin-histochemistry

Lectin histochemistry was performed as previously described [52]. Slides were washed with Tris-buffered saline supplemented with Ca^{2+} and Mg^{2+} (TBS; 20 mM Tris-HCl, 100 mM NaCl, 1 mM $CaCl_2$, 1 mM $MgCl_2$, pH 7.2) and 0.05% (v/v) Triton X-100 (TBS-T), then blocked with 2% (w/v) periodate-treated BSA in TBS for 1 h. All experiments were performed in darkness and all washes (5 min each) were carried out three times. Sections were washed, then incubated with FITC-conjugated lectins (WGA, SNA-I, GNA (EY Labs, United States)) in TBS for 1 h. After three washes with TBS-T, the sections were counterstained with a 1:1000 dilution of DAPI for 5 min. The slides were washed in TBS-T before coverslip mounting with ProLong® Gold Antifade Mountant (Life Technologies). All slides were incubated at 4 °C in darkness for 24 h before imaging with a laser confocal microscope (Olympus Fluoview 1000, Olympus America, Center Valley, PA, USA).

4.7. Morphometry

Stereological quantification was adopted to measure angiogenesis, arteriogenesis, fibrosis, inflammation, and the lectin binding to the specific glycans following a published method [52–54]. For angiogenesis, capillary density, length density and radial diffusion were quantified. For arteriogenesis, the arterioles density and cross section area was measured. The volume fraction of collagen deposition (fibrosis), infiltrating inflammatory cells, CD163+ cells and detectable lectin binding to the glycans was also evaluated. ImageJ software version 1.48 [National Institutes of Health (NIH)] was used for all stereological quantifications.

1. Capillary and density, length density and radial Diffusion

Confocal images of CD31 immunological staining (20X) were used to determine capillary density, length density and radial diffusion. The points where the squares on the grid intersected blood vessels are numbered on the section. The surface capillary density of blood vessels was calculated using the intersected blood vessels multiplied by the area of the square. The total length of blood vessels in the muscle was calculated by multiplying length density (L) by volume of the muscle. Radial diffusion was calculated using formula (1/Square root (L*Pi)), which is the distance between blood vessels and is an indicator of the

capillary network in the vascular bed. The shorter the distance between blood vessels, the smaller the distance required for nutrients to diffuse into surrounding tissues.

2. Arterioles density and cross section area.

Confocal images of αSMA immunological staining (20X) were used to determine arterioles density, and their cross section area. Four stereological grids were superimposed on each image to quantify either arterioles density per squared mm (i.e. the objects of interest falling inside the grids were counted to get the numerical estimates) To measure the area of the arterioles cross sections, a total of 30 arterioles per group were measured.

3. Volume fraction of collagen deposition/fibrosis

Collagen deposition and subsequent fibrosis were measured through Masson's trichrome staining following the manufacturer's instructions on the kit (HT15, Sigma). Images were acquired in a VS120 virtual slide microscope (Olympus, Japan) at 20x magnification. For quantification of fibrosis, a grid made of 228 points was superimposed on each image taken. The volume fraction percentage (Vv%) of inflammatory cells was calculated using the formula: Number of grid points hitting collagen fibres/total number of grid points X100.

4. Volume fraction of inflammatory cells and CD163+ cells

H&E stained sections were imaged on an Olympus slide scanner microscope. Images were taken at 40X magnification. Confocal images of *CD163* immunological staining (20X) were used to determine arterioles density, and their cross section area. The volume fraction of infiltrating inflammatory cells was also evaluated. Inflammatory cells were counted and these cells included lymphocytes and neutrophils. The volume fraction was determined with a 528-point grid using ImageJ software. Neutrophils were identified as small dense circular multilobed cells and lymphocytes as small round dense cells with large nuclei. The volume fraction percentage (Vv%) of inflammatory cells was calculated using the formula: Number of cells intersecting the grid points/total number of grid points X100.

5.Volume fraction of lectin-binding glycans

A stereology method was used to calculate the percentage volume fraction of the detectable lectin binding to specific glycans. Volume fraction was calculated according to a previously described method [52]. Confocal images were converted to binary mode (8 bits) and adjusted to the optimal threshold of positive staining and total area using ImageJ software version. Volume fraction was calculated by quantifying the area fraction of the positively stained tissue divided by the total area and converting this into a percentage (%): percentage volume fraction (%Vv) = Area Fraction of the signal/Total Area x 100.

4.8. Raman microspectroscopy

Tissue sections on a glass slide were analyzed using a custom-built Raman microspectroscopy system as previously described [55]. Briefly, all measurements were performed using a 60X water immersion objective (NA 1.2, Olympus). Using an automated stage, 30 spectra were collected in the ECM surrounding single muscle fibers. Raman spectra were acquired in the wavenumber range of 0–2000 cm^{-1} using an acquisition time of 100 s with 85 mW laser power. Spectra were recorded using the Andor software package (Andor iDus, Belfast, Northern Ireland). OPUS®software 4.2 (Bruker Optik GmbH, Ettlingen, Germany), was used to subtract the glass background signals and as well to cut the Raman spectra into the spectral 400–1800 cm^{-1} region. After baseline correction, all Raman spectra were imported to the UnscramblerX® 10.2 Software (CAMO, Oslo, Norway). Principal component analysis (PCA) was used to analyze the spectra. PCA is a multivariate method utilized to analyze the variances in a spectral dataset and is useful to identify significant shifts in the spectra between sample groups. The non-linear iterative partial squares (NIPALS) algorithm was used in the calculation of PCA. As a result of the PCA, every spectrum is described by score values. Separation of score plots reveals differences between sample groups, while loadings highlight the peaks of the spectra that are responsible for the differences.

4.9. Fluorescent labelling of glycoproteins

Healthy, not treated (PBS), and ELRs treated tissues were homogenized and resuspended in RIPA buffer (Thermo Fischer Scientific). Protein samples from nine biological replicates per group were pooled together and analyzed as a single replicate.

Protein fraction (1 mg) and asialofetuin (ASF) were fluorescently labelled with Alexa Fluor® 647 (carboxylic acid succinimidyl ester, excitation 650 nm, λ emission 665 nm) in 100 mM sodium bicarbonate, pH 8.0 for 1 h in the dark essentially as previously described [51]. Excess dye was removed from the labelled samples using a centrifugal desalting column (7 kDa MWCO). Absorbance at 650 and 280 nm for each sample was measured and the protein concentration and degree of substitution were determined according to manufacturer's instructions using the extinction coefficient 85.700 M−1 cm−1.

4.10. Lectin microarray profiling

The lectin microarray (Table S9) was constructed essentially as previously described. All samples were incubated on microarray slides in triplicate essentially as previously described [56]. Fluorescently-labelled samples and ASF control were diluted to 0.5 μg/ml in Tris-buffered saline (TBS) supplement with 0.05% Tween-20 (TBS-T2). The slides were imaged immediately in an Agilent G2505 microarray scanner using the Cy5 channel (633 nm excitation, 80% PMT, 5 μm resolution).

Raw intensity values were extracted from the image files using GenePix Pro v6.1.0.4 (Molecular Devices, Berkshire, U.K.) and data was processed essentially as previously described [50]. Local background-corrected median feature intensity data (F543median-B543) was selected and the median of six replicate spots per subarray was considered as a single data point.

4.11. Proteomic analysis by LC-MS/MS

Quadriceps biopsies have been snap-frozen and preserved for mass spectrometry analysis. 50 mgs of quadriceps were homogenized in 1 ml of RIPA buffer and 10% of proteases inhibitor cocktail (PIC) using a tissue homogenizer Tissue Lyser LT (Qiagen, UK). Proteins from 9 animals per group were pooled in one replicate. The proteins were reduced in 2% sodium dodecyl sulfate (SDS) at 60 °C for 30 min and alkylated in N-Ethylmaleimide (NEM) (Thermo Fisher Scientific) in the dark at 37 °C for 30 min. After precipitation in methanol-chloroform, the pellet was dried and re-dissolved in 100 μl of 8 M urea in 0.1 M TEAB (0.96 g/2 ml). The samples were digested in trypsin (10 μg in 50 mM acetic acid) (Sigma Aldrich) at 37 °C overnight with shaking. Digestion was stopped by adding 1% trifluoroacetic acid (TFA) (Sigma Aldrich) in LC-grade water. Tryptic-digested peptides were washed by SEP-Pak C18 cartridge (Millipore), pre-washed with methanol. After loading the sample, the C18 cartridge was rinsed with 0.1% TFA. The peptide concentration in the samples was determined after digestion and desalting using the Thermo Scientific™ Pierce™ Quantitative Colorimetric Peptide Assay. Peptides were resuspended in 0.1 M TEAB at a concentration of 2 μg/μl to normalize the volumes for the Tandem mass tag (TMT) labelling. The Thermo Scientific™ TMT Labeling Kits and Reagents were used to do multiplex relative quantification by mass spectrometry (MS) of the

processed samples. After the labelling procedure, peptides were dissolved in 500 μl 1% TFA and cleaned up again in the SEP-Pak C18 cartridge. After determination of the concentration, the samples were fractionated into 4 fractions by offline High pH reversed phase chromatography. Each fraction was loaded into a reversed phase column, eluted over a 2.5 h gradient and injected by ESI on a Fusion Tribrid Orbitrap instrument operating in data dependent acquisition (top-12) mode. Acquired raw spectra files were searched in MaxQuant against a FASTA mouse reference proteome database from UniProt. MaxQuant output results were loaded in R for further analysis. MaxQuant output results were uploaded in R for further analysis. Protein groups were filtered to exclude: proteins identified with only 1 peptide (dubious identifications), common contaminants, decoy database hits, and proteins identified only by post-translationally modified site. Protein-level estimates of expression and ratios between the different conditions were re-calculated using the healthy control as reference and the estimated relative abundance was expressed as log2 fold change. Proteins of interest were filtered according to the following criteria: 1) quantitative values present for all the time points and groups 2) the maximum fold change for the protein group is at least 1.5.

4.12. Ingenuity Pathway Analysis

Ingenuity Pathway Analysis (IPA) software was used to perform pathway analysis, from information contained in the IPA knowledge base (IPKB). Protein expression comparison between the injury and ELR hydrogel groups was conducted. For this purpose, the −log (p value) threshold was set to 1.3 to determine dysregulated biological functions. Activated pathways and upstream regulators related to the relevant biological function were analyzed through z-score to be activated or inhibited.

4.13. N-glycan analysis via LC-ESI-MS/MS

The extracted protein fractions (n = 4, for phase II, n = 5–8 for phase III) were filtered (30 kDa-cutoff). The filter was washed in 200 μl of 7 M urea (3X), 2 M thiourea and 40 mMTris-HCl. The samples were reduced in 25 mM Dithiothreitol (DTT) overnight at 4 °C. After incubation in 2.5-fold iodoacetamide (Sigma Aldrich) in the dark for 1 h at room temperature, the samples were digested with trypsin (1 μg) at 37 °C overnight, as previously described [57]. The obtained digested peptides were precipitated with 80% acetone, air-dried and digested with PNGase F enzyme in 50 mM NH_4Ac (pH 8.4). This step ensures the release of glycans from the proteins. The samples were incubated at 37 °C overnight. N-glycans were separated from O-glycopeptides/polypeptides by SEP-Pak C18 cartridge (Waters corporation), and pre-washed with methanol. After loading the sample, the C18 cartridge was rinsed with 0.1% TFA. The released N-glycans, contained in the eluted fractions, were dried in a SpeedVac and reduced by using 0.5 M $NaBH_4$ in 10 mM NaOH at 50 °C overnight. The samples were desalted using cation exchange resin (AG50W x 8) packed onto a ZipTip C18 tip (Millipore). Additional methanol was added to remove residual borate by evaporation. The resultant N-glycans have been analyzed by LC-MS/MS as described [58]. The oligosaccharides were separated on a column (10 cm × 250 μm) packed in-house with 5 μm porous graphite particles (Hypercarb, Thermo-Hypersil, Runcorn, UK). The oligosaccharides were injected into the column and eluted with an acetonitrile gradient (Buffer A, 10 mM ammonium bicarbonate; Buffer B, 10 mM ammonium bicarbonate in 80% acetonitrile (Sigma Aldrich)). The gradient (0–45% Buffer B) was eluted for 46 min, followed by a wash step with 100% Buffer B, and equilibrated with Buffer A for 24 min. A 40 cm × 50 μm i.d. fused silica capillary was used as a transfer line to the ion source.

The samples were analyzed in negative ion mode on an LTQ linear ion trap mass spectrometer (Thermo Electron, San José, CA), with an IonMax standard ESI source equipped with a stainless steel needle kept at −3.5 kV. Compressed air was used as nebulizer gas. The heated capillary was kept at 270 °C, and the capillary voltage was −50 kV. Full scan (*m/z* 380–2000, two microscans, maximum 100 ms, target value of 30,000) was performed, followed by data-dependent MS [2] scans (two microscans, maximum 100 ms, target value of 10,000) with normalized collision energy of 35%, isolation window of 1.0 units, activation q = 0.25 and activation time 30 ms). The threshold for MS [2] was set to 300 counts. Data acquisition and processing were conducted with Xcalibur software (Version 2.0.7).

Glycans were identified from their MS/MS spectra by manual annotation. For structural annotation, some assumptions were made in this study as follows. The biosynthesis of N-glycans was assumed to follow the classic pathways. Terminal Hex_2 units were presumed to be αGal. Chain elongation was expected to be mediated by the addition of N-acetyllactosamine units. Diagnostic fragmentation ions for N- and O-glycans were investigated as described [58]. The annotated structures according to MIRAGE guideline were submitted to the UniCarb-DR repository (https://unicarb-dr.glycosmos.org/references/364). For comparison of glycan abundances between samples, individual glycan structures were quantified relative to the total content by integration of the extracted ion chromatogram peak area. The area under the curve (AUC) of each structure was normalized to the total AUC and expressed as a percentage. The peak area was processed by Progenesis QI (Nonlinear Dynamics, Newcastle, UK). The row files containing the peaks intensity are available at the following link (https://glycopost.glycosmos.org/preview/5608636085cb07abf3cda4, code 3354).

5. Statistical analysis

Statistical evaluation of the data was performed using the statistical program GraphPad Prism® Version 5 (USA); data were compared using one-way ANOVA and two-way ANOVA where appropriate. ANOVA tests were further evaluated with a Tukey post-hoc comparison test. All data were expressed as mean ± standard deviation. Significance was accepted at p-value < 0.05.

CRediT author statement

G.M designed, performed, and analyzed the experiments and wrote the manuscript. J.M assisted in analyzing MS data and contributed to discuss the glycomic data, S.A.A performed the surgeries in the animal study and assisted in the manuscript writing. E.B. contributed in analyzing and discussing Raman analysis. D.T designed the animal model and contributed to Doppler analysis. A.L.R performed macrophage, collagen and arterieles imaging and quantication. D.O designed the ELRs, S.C analyzed the GAGs P.C assisted in the animal studies. D.P guided and discussed the GAGs studies. C.R.C designed and provided the ELRs. M.K performed the lectin microarray analysis and discussed the results. K.S.L directed and discussed Raman study. N.G.K guided and discussed the glycomics study, K.M.C guided histology and stereology quantification and discussed the results, A.P. directed the project, designed all the experiments and discussed the results. AP received the grants for the project. All the authors have contributed towards the preparation and approved the final version the manuscript

Declaration of competing interest

The authors declare that they have no known competing financial interests or personal relationships that could have appeared to influence the work reported in this paper.

Acknowledgements

General: We thank Mr Ruben Daum and Mr Daniel Alejandro Carvajal Berrio (both of the Dept. of Women's Health, University of Tübingen) for their support in Raman microspectroscopy. We thank Prof. Peter Dockery, and Dr Kerry Thompson and Mr Mark Canney from

the Anatomy Department, NUI Galway for their advice and assistance. We thank Prof. Fabio Quondamatteo for his guidance and advice and Dr Aniket Kshirsagar and Dr Isma Liza Mohd Isa for their help in interpreting proteomics analysis, and Ms Jaspreet Kaur for the assistance with histology. We also acknowledge the editorial assistance of Mr Anthony Sloan and Dr Raghvendra A. Bohara, and the graphic design support of Mr Maciek Dozkyk. We are grateful as well for the laboratory technical support provided by Dr Oliver Carroll at the CÚRAM SFI Research Centre for Medical Devices.

Appendix A. Supplementary data

Supplementary data to this article can be found online at https://doi.org/10.1016/j.biomaterials.2020.120641.

Funding

This work was funded by Science Foundation Ireland (SFI) and the European Regional Development Fund (Grant Number 13/RC/2073) AngioMatTrain Seventh Framework Programme Grant Agreement no.: 317304. The authors acknowledge the core-facilities and technical assistance of the Centre for Microscopy and Imaging (CMI), funded by the National University of Ireland, Galway and the Irish Government's Programme for Research in Third Level Institutions, Cycles 4 and 5, National Development Plan 2007–2013. Research in the Raman microspectroscopy laboratory was supported by DAAD Boehringer Ingelheim Fonds travel grant [2016, to MG], by the Peter and Traudel Engelhorn foundation (Postdoc fellowship to EMB) as well as by the Deutsche Forschungsgemeinschaft (INST 2388/64-1, INST 2388/30-1) and the Ministry of Science, Research and Arts of Baden Württemberg (Az.: SI-BW 01222-91, 33-729.55-3/214) [all to KS-L]. Research in the mass spectrometry laboratory at the University of Goteborg was supported by EMBO short-term fellowships [ASTF- 7602-2018] in collaboration with the Swedish infrastructure for biological mass spectrometry (BioMS) supported by the Swedish Research Council.

References

[1] M. Teraa, M.S. Conte, F.L. Moll, M.C. Verhaar, J Am Heart Assoc 5 (2016) 2.
[2] B.H. Annex, Nat. Rev. Cardiol. 10 (2013) 387.
[3] D. Thomas, A. Thirumaran, B. Mallard, X. Chen, S. Browne, A.M. Wheatley, T. O'Brien, A. Pandit, Tissue Eng Part C Methods. 22 (2016) 370.
[4] H. Kolarova, B. Ambruzova, L. Svihalkova Sindlerova, A. Klinke, L. Kubala, Modulation of conditions, Mediat. Inflamm. (2014) 694312.
[5] R.L. Schnaar, J. Leukoc. Biol. 99 (2016) 825.
[6] R.D. Wright, D. Cooper, Glycobiology 24 (2014) 1242.
[7] P. Chiodelli, S. Rezzola, C. Urbinati, F. Federici Signori, E. Monti, R. Ronca, M. Presta, M. Rusnati, Oncogene 36 (2017) 6531.
[8] D.O. Croci, J.P. Cerliani, T. Dalotto-Moreno, S.P. Mendez-Huergo, I. D. Mascanfroni, S. Dergan-Dylon, M.A. Toscano, J.J. Caramelo, J.J. Garcia-Vallejo, J. Ouyang, E.A. Mesri, M.R. Junttila, C. Bais, M.A. Shipp, M. Salatino, G. A. Rabinovich, Cell. 156 (2014) 744.
[9] R.A. Peattie, Curr. Pharmaceut. Biotechnol. 13 (2012) 1299.
[10] B.C. Dash, D. Thomas, M. Monaghan, O. Carroll, X. Chen, K. Woodhouse, T. O'Brien, A. Pandit, Biomaterials 65 (2015) 126.
[11] D. Thomas, G. Fontana, X. Chen, C. Sanz-Nogues, D.I. Zeugolis, P. Dockery, T. O'Brien, A. Pandit, Biomaterials 35 (2014) 8757.
[12] G. Milcovich, P. Contessotto, G. Marsico, S. Ismail, A. Pandit, Sci. Rep. 1 (2017) 13138.
[13] R. Spelat, F. Ferro, P. Contessotto, N.J. Warren, G. Marsico, S.P. Armes, A. Pandit, Mater Today Bio. 5 (2020) 100040.
[14] D. W Urry, Prog. Biophys. Mol. Biol. 57 (1992) 23.
[15] S. M Mithieux, Anthony S. Weiss, Adv. Protein Chem. 70 (2005) 61.
[16] J. Cappello, J. Crissman, M. Dorman, M. Mikolajczak, G. Textor, M. Marquet, F. Ferrari, Biotechnol. Prog. 6 (1990) 198.
[17] T. Yamaoka, T. Tamura, Y. Seto, T. Tada, S. Kunugi, D.A. Tirrell, Biomacromolecules 4 (2003) 1680.
[18] A. Fernández-Colino, F.J. Arias, M. Alonso, J.C. Rodríguez-Cabello, Biomacromolecules 16 (2015) 3389.
[19] T. Flora, I.G. de Torre, M. Alonso, J.C. Rodriguez-Cabello, J. Mater. Sci. Mater. Med. 30 (2019) 30.
[20] S.M. Staubli, G. Cerino, I. Gonzalez De Torre, M. Alonso, D. Oertli, F. Eckstein, K. Glatz, J.C. Rodriguez Cabello, A. Marsano, Biomaterials 135 (2017) 30.
[21] B.J. McMorran, F.E. McCarthy, E.M. Gibbs, M. Pang, J.L. Marshall, A.V. Nairn, K. W. Moremen, R.H. Crosbie-Watson, L.G. Baum, Glycobiology 26 (2016) 1120.
[22] B.L. Parker, G. Palmisano, A.V. Edwards, M.Y. White, K. Engholm-Keller, A. Lee, N. E. Scott, D. Kolarich, B.D. Hambly, N.H. Packer, M.R. Larsen, S.J. Cordwell, Mol. Cell. Proteomics 10 (2011) 110.
[23] D. Liu, Z. Zhao, A. Wang, S. Ge, H. Wang, X. Zhang, Q. Sun, W. Cao, M. Sun, L. Wu, M. Song, Y. Zhou, W. Wang, Y. Wang, Neuroinflammation 15 (2018) 123.
[24] G. Wang, M.R. de Vries, W. Sol, A.M. van Oeveren-Rietdijk, H.C. de Boer, A.J. van Zonneveld, P. Quax, T.J. Rabelink, B.M. van den Berg, Cells 9 (2020) 824.
[25] I. Loke, D. Kolarich, N.H. Packer, M. Thaysen-Andersen, Mol. Aspect. Med. 51 (2016) 31.
[26] B.K. Chacko, D.W. Scott, R.T. Chandler, R.P. Patel, J. Biol. Chem. 286 (2011) 38738.
[27] T. Isaji, Y. Kariya, Q. Xu, T. Fukuda, N. Taniguchi, J. Gu, Methods Enzymol. 480 (2010) 445.
[28] A.B. Katwal, P.R. Konkalmatt, B.A. Piras, S. Hazarika, S.S. Li, R. John Lye, J. M. Sanders, E.A. Ferrante, Z. Yan, B.H. Annex, B.A. French, Gene Ther. 20 (2013) 930.
[29] F. Chevalier, D. Arnaud, E. Henault, O. Guillevic, F. Sineriz, A.C. Ponsen D. Papy-Garcia, D. Barritault, D. Letourneur, G. Uzan, A. Meddahi-Pelle, H. Halawaty, P. Albanese, European Cells &Mat Journal 30 (2015) 51.
[30] F. Corti, Y. Wang, J.M. Rhodes, D. Atri, S. Archer-Hartmann, J. Zhang, Z. W. Zhuang, D. Chen, T. Wang, Z. Wang, P. Azadi, M. Simons, Nat. Commun. 10 (2019) 1562.
[31] S. Hinderer, S.L. Layland, K. Schenke-Layland, Adv. Drug Deliv. Rev. 97 (2016) 260.
[32] J. Cao, M. Ehling, S. Marz, J. Seebach, K. Tarbashevich, T. Sixta, M.E. Pitulescu, A. C. Werner, B. Flach, E. Montanez, E. Raz, R.H. Adams, H. Schnittler, Nat. Commun. 8 (2017) 2210.
[33] B.A. Bryan, P.A. D'Amore, Cell. Mol. Life Sci. 64 (2007) 2053–2065.
[34] A. Robinet, A. Fahem, J.H. Cauchard, E. Huet, L. Vincent, S. Lorimier, F. Antonicelli, C. Soria, M. Crepin, W. Hornebeck, G. Bellon, J. Cell Sci. 118 (2005) 343.
[35] P.R. Somanath, A. Ciocea, T.V. Byzova, Cell Biochem. Biophys. 53 (2009) 53.
[36] K. Gaengel, G. Genove, A. Armulik, C. Betsholtz, Arterioscler. Thromb. Vasc. Biol. 29 (2009) 630.
[37] M. Bartoli, X. Gu, N.T. Tsai, R.C. Venema, S.E. Brooks, M.B. Marrero, R.B. Caldwell, J Biol Chem 275 (2000) 33189.
[38] M. Murakami, M. Simons, Curr. Opin. Hematol. 15 (2008) 215.
[39] E. Brauchle, J. Kasper, R. Daum, N. Schierbaum, C. Falch, A. Kirschniak, T. E. Schaffer, K. Schenke-Layland, Matrix Biol. 180 (2018) 68.
[40] A. Neve, F.P. Cantatore, N. Maruotti, A. Corrado, D. Ribatti, BioMed Res Int. 2014 (2014) 756078.
[41] M. Mongiat, E. Andreuzzi, G. Tarticchio, A. Paulitti, Int. J. Mol. Sci. 17 (2016) 1822.
[42] A. Ibáñez-Fonseca, S. Santiago Maniega, D. Gorbenko del Blanco, B. CatalánBernardos, A. Vega Castrillo, Á.J. Álvarez Barcia, M. Alonso, 1, H. J. Aguado, J.C. Rodríguez-Cabello, Front Bioeng Biotechnol 8 (2020) 413.
[43] S. Browne, M.G. Monaghan, E. Brauchle, D.C. Berrio, S. Chantepie, D. Papy-Garcia, K. Schenke-Layland, A. Pandit, Biomaterials 69 (2015) 133.
[44] D. Thomas, G. Marsico, I.L. Mohd Isa, A. Thirumaran, X. Chen, B. Lukasz, G. Fontana, B. Rodriguez, M. Marchetti-Deschmann, T. O'Brien, A. Pandit, Proc. Natl. Acad. Sci. U. S. A. 117 (2020) 19033.
[45] E. Chiffoleau, Front. Immunol. 9 (2018) 227.
[46] B.K. Chacko, D.W. Scott, R.T. Chandler, R.P. Patel, J. Biol. Chem. 286 (2011) 38738.
[47] A. Varki, Biological roles of glycans, Glycobiology 27 (2017) 3.
[48] G. Marsico, L. Russo, F. Quondamatteo, A. Pandit, Trends Cancer 8 (2018) 537.
[49] S. Abraham, M. Scarcia, R.D. Bagshaw, K. McMahon, G. Grant, T. Harvey, M. Yeo, F.O.G. Esteves, H.H. Thygesen, P.F. Jones, V. Speirs, A.M. Hanby, P.J. Selby, M. Lorger, T.N. Dear, T. Pawson, C.J. Marshall, G. Mavria, Nat. Commun. 6 (2015) 7286.
[50] S. Kanda, Y. Miyata, H. Kanetake, T.E. Smithgall, Int. J. Mol. Med. 20 (2007) 113.
[51] I. Gonzalez de Torre, M. Santos, L. Quintanilla, A. Testera, M. Alonso, J.C. Cabello, Acta Biomater. 10 (2014) 2495.
[52] P. Contessotto, B.W. Ellis, C. Jin, N.G. Karlsson, P. Zorlutuna, M. Kilcoyne, A. Pandit, Matrix Biol. 85 (2019) 173.
[53] Y. Garcia, A. Breen, K. Burugapalli, P. Dockery, A. Pandit, Biomaterials 28 (2007) 175–186.
[54] L.M. Cruz-Orive, J. Anat. 194 (1999) 153.
[55] M. Pudlas, S. Koch, C. Bolwien, S. Thude, N. Jenne, T. Hirth, H. Walles, K. Schenke-Layland, Tissue Eng. C Methods 17 (2011) 1027.
[56] B.A. Abhari, N. McCarthy, M. Le Berre, M. Kilcoyne, L. Joshi, P. Agostinis, S. Fulda, Cell Death Dis. 10 (2019) 155.
[57] P.H. Jensen, N.G. Karlsson, D. Kolarich, N.H. Packer, Nat. Protoc. 7 (2012) 1299.
[58] A.V. Everest-Dass, J.L. Abrahams, D. Kolarich, N.H. Packer, M.P. Campbell, Structural feature ions for distinguishing N- and O-linked glycan isomers by LC-ESI-IT MS/MS, J. Am. Soc. Mass Spectrom. 24 (2013) 895.